Control of boundary slip by interfacial nanobubbles: A perspective from molecular dynamics simulations

Haichang Yang (杨海昌) ; Binglin Zeng (曾炳霖) ; Xuehua Zhang (张雪花) ; Yaowen Xing (邢耀文) ;
Xiahui Gui (桂夏辉); Yijun Cao (曹亦俊)

Check for updates

CrossMark

View Online

Export Citation

Physics of Fluids

Special Topic:

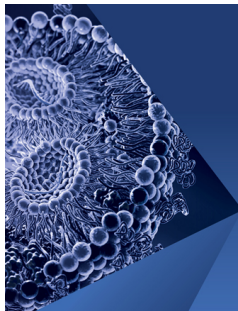**Flow and Lipid Nanoparticles**

Guest Editors: Richard Braatz and Mona Kanso

Submit Today!

AIP Publishing

Control of boundary slip by interfacial nanobubbles: A perspective from molecular dynamics simulations

View Online   Export Citation   CrossMark

Haichang Yang (杨海昌),[1,2,3] (iD) Binglin Zeng (曾炳霖),[2] (iD) Xuehua Zhang (张雪花),[2] (iD) Yaowen Xing (邢耀文),[1,a)] Xiahui Gui (桂夏辉),[1] and Yijun Cao (曹亦俊)[1,4,a)]

AFFILIATIONS

[1]National Engineering Research Center of Coal Preparation and Purification, China University of Mining and Technology, Xuzhou 221116, Jiangsu, China
[2]Department of Chemical and Materials Engineering, University of Alberta, Edmonton, Alberta T6G 1H9, Canada
[3]School of Chemical Engineering and Technology, China University of Mining and Technology, Xuzhou 221116, Jiangsu, China
[4]School of Chemical Engineering and Technology, Zhengzhou University, Zhengzhou 450066, Henan, China

[a)]Authors to whom correspondence should be addressed: cumtxyw@126.com and yijuncao@126.com

ABSTRACT

Enhancing boundary slip using interfacial nanobubbles (INBs) has gained significant interest in nanofluidic transport. In this study, we conducted a comprehensive investigation on the influence of INBs on boundary conditions for both smooth and rough substrates using molecular dynamics simulations. We analyzed the impact of INB protrusion angle, coverage percentage, quantity, and fluidity on the slip length. Our results showed that INBs always increase the slip length on a smooth substrate, with a linear increase in slip length observed with increasing surface coverage. On a rough substrate, we found that the protrusion angle, quantity, and fluidity of INBs play a crucial role in determining the slip length. Smaller protrusion angles and fewer quantities of INBs were found to be more favorable for enhancing the slip length when the INB coverage is fixed, while the correlation between boundary slip and INB quantity depended on the wetting state of the substrate when the size of the INBs was fixed with a low protrusion angle. Additionally, we revealed that the fluidity of gas molecules inside the INBs dominated the enhancement of slip length by INBs. Overall, our findings are expected to provide valuable insight into drag reduction based on INBs.

Published under an exclusive license by AIP Publishing. https://doi.org/10.1063/5.0141614

I. INTRODUCTION

When water flows near a wall, it suffers frictional drag from the surface, resulting in a declining shear flow velocity from bulk to the solid–liquid interface. For macro-scale systems, the shear flow velocity at the solid–water interface is commonly assumed to be zero, a condition known as the no-slip boundary condition.[1,2] However, the exact boundary condition at the solid–liquid interface is crucial for accurately calculating the flow behavior. In nanofluidic systems, the no-slip boundary condition is no longer practical.[1,3] In recent decades, experimental evidence has demonstrated the existence of slip boundary conditions on both hydrophilic[4,5] and hydrophobic[6–8] surfaces. The presence of slippage reduces energy dissipation in liquid transport,[9] making it crucial for many applications, such as micro-fluidics,[10–12] mineral flotation,[13,14] fish flapping motion,[15] gas-liquid filtration,[16–18] and shear in colloidal suspensions.[19] The strength of the boundary slip is typically quantified by the slip length, which was first proposed by

Navier.[20] The slip length is defined as the distance below the solid–liquid interface at which the liquid velocity linearly extrapolates to zero. A longer slip length indicates a stronger boundary slip, which corresponds to a smaller frictional drag from the solid surface.

Interfacial nanobubbles (INBs) have been demonstrated to be able to enhance the boundary slip both theoretically[21–23] and experimentally.[2,24,25] INB is usually defined as a cap-shaped gas bubble with a height of less than 1 μm. INB has several unique properties, including ultra-low contact angle (from the gas side),[26–29] long-term stability,[27,30–32] and high gas density.[33–35] Vega-Sánchez *et al.*[2] reported that the slip length is longer when using high-gas-content water than degassed water. With the employment of atomic force microscopy, Vega-Sánchez *et al.*[2] further revealed that INBs are responsible for this enhanced boundary slippage. For a continuous gas film existing between the solid–liquid interface, the slip length is suggested as[36,37]

$$b = h_0 \left(\frac{\mu_w}{\mu_g} - 1 \right), \qquad (1)$$

where h_0 is the thickness of the gas film, and μ_w and μ_g are the viscosity of the water and gas layer, respectively. The ratio of μ_w and μ_g is about 55.[38] For INB-covered substrates, the INBs are discretely distributed over the surface rather than acting as a continuous gas film. Considering this, Wang *et al.*[39] proposed that the h_0 should be replaced with $h_0 = h_b \phi$, where h_b and ϕ are the height and coverage percentage of INBs. Therefore, the equation of slip length is developed as follows:[39]

$$b = \left(\frac{\mu_w}{\mu_g} - 1 \right) h_b \phi. \qquad (2)$$

Li *et al.*[40] studied the correlation between INBs and slip length. When the coverage percentages of INBs were 1.7%, 4.8%, 15.5%, and 50.8%, the slip lengths were measured as 8, 21, 85, and 512 nm, respectively. It was found that the calculated slip lengths by Wang *et al.*'s[39] model [Eq. (2)] were overestimated compared with the measured ones. They thought the reason was the neglect of the INB morphology. By adding the term of INB protrusion angle, the equation of slip length is further developed as

$$b = \left(\frac{\mu_w}{\mu_g} - 1 \right) \left(\frac{h_b}{2} + \frac{h_b}{6} \tan^2 \frac{\theta}{2} \right) \phi, \qquad (3)$$

where θ is the protrusion angle of the INB. With Eq. (3), the theoretical slip length fitted the experimental results well. Although amounts of experiments proved that the INBs can increase the slip length, sometimes, the bubbles may inhibit the boundary slip.[22,41,42] To date, the microscopic mechanism of INBs acting on liquid flow has not been fully revealed.

Simulation is a powerful tool to study the microscopic behavior of the flow and the mechanism behind the enhancement of boundary slip by INBs.[43–47] By the finite-element method, both Steinberger *et al.*[43] and Karatay *et al.*[25] numerically found a negative relationship between the slip length and the protrusion angle of INBs. With the molecular dynamics (MD) simulations, Lu[46] investigated the synergistic effect of INBs, with surface hydrophobicity and flow velocity on the slip length. The author concluded that the high hydrophobicity of the substrate coupled with the high flow rate results in a significant drag reduction by INBs. Cottin-Bizonne *et al.*[48] simulated the boundary conditions in a nanochannel and found that the combined effect of the Cassie–Baxter wetting state and surface roughness considerably reduced the friction drag.

In this study, we used molecular dynamics (MD) simulations to investigate the impact of interfacial nanobubbles (INBs) on boundary conditions for substrates with different hydrophobicities and roughness. Specifically, we conducted nonequilibrium Couette flow simulations to calculate the slip length on various surfaces. In our simulations, the bottom surface was held at a fixed position, while the top surface was pulled along the X direction with a constant velocity of 20 m/s. We analyzed the flow fields of water molecules outside the INBs and gas molecules inside the INBs. We systematically studied the dependence of the slip length on the surface hydrophobicity, INB coverage, protrusion angle, quantity, and fluidity of INBs. Our results indicate that surface hydrophobicity, INB coverage, and quantity

influence the magnitude of the slip length, while the protrusion angle and fluidity of INBs determine the sign of the slip length. Additionally, we found that the fluidity of INBs dominates the enhancement of the boundary slip. Our study provides a new perspective in understanding drag reduction by INBs in both fundamental and applied aspects.

II. SIMULATION METHODOLOGY

A. Simulation settings

Open-source GROMACS 2019.6 software[49] was used to perform MD simulations in this work. The interactions between atoms were based on a combination of Lennard-Jones (LJ) 6–12 potential and Coulomb potential,

$$U(r_{ij}) = 4\varepsilon_{ij} \left(\left(\frac{\sigma_{ij}}{r_{ij}} \right)^{12} - \left(\frac{\sigma_{ij}}{r_{ij}} \right)^{6} \right) + f \frac{q_i q_j}{r_{ij}}, \qquad (4)$$

$$\sigma_{ij} = \sqrt{\sigma_{ii} \sigma_{jj}}, \qquad (5)$$

$$\varepsilon_{ij} = \sqrt{\varepsilon_{ii} \varepsilon_{jj}}, \qquad (6)$$

where ε_{ij} is the LJ potential well depth between atoms i and j; σ_{ij} is the characteristic size; r_{ij} is the distance between atoms i and j; q_i and q_j are the charges of atoms i and j, respectively; f is the electric conversion factor with a value of 138.935 458 kJ mol^{-1} nm e^{-2}.

Periodic boundary conditions were applied in the x and y directions, as shown in Fig. 1(a) (Multimedia view). For all equilibration and production simulations, the leap-frog algorithm was used for integrating Newton's equations of motion. The time step was 2.0 fs. The trajectory file was output every 1000 steps. VMD 1.9.3 software[50] was used for the visualization of the trajectory. The coulomb type was fast smooth particle-mesh Ewald electrostatics (PME), where the direct space was similar to the Ewald sum, while the reciprocal part was performed with FFTs. Both the cutoff radii for LJ interactions and the real space of electrostatic interaction were 1.2 nm. The V-rescale thermostat was used for the temperature coupling, and the fluid temperature was always set at 298.15 K. The widely used SPC/E water model was employed to simulate water molecules. A two-site nitrogen model (bond length = 0.112 nm) was used as the gas molecule.[51,52] Three or eight graphene layers (bond length = 0.142 nm) were used as the solid substrate. The interaction parameters of each atom type in the current work are listed in Table I, where S_T represents the top slab whose contact angle was zero, S_1, S_2, S_3, S_4, and S_5 are used to represent substrates with different hydrophobicities, whose contact angles are 36°, 66°, 90°, 115°, and 124°, respectively, O_W and H_W represent oxygen and hydrogen atoms of the water molecule, and N is the nitrogen atom of the nitrogen molecule.

B. Simulation procedures

To simulate the boundary conditions of the substrate, a slab was placed at the top of the water phase. The initial model was constructed by using the built-in command in GROMACS, combined with Packmol,[53] VMD,[50] and Python script. Energy minimization was conducted before running the simulations. The steepest descent algorithm was used in the energy minimization process. The energy minimization was converged when the maximum force was smaller than 300.0 kJ mol^{-1} nm^{-1}.

After energy minimization, we started the equilibrium stage. In this stage, a downward pressure of 1 bar was imposed on the top slab.
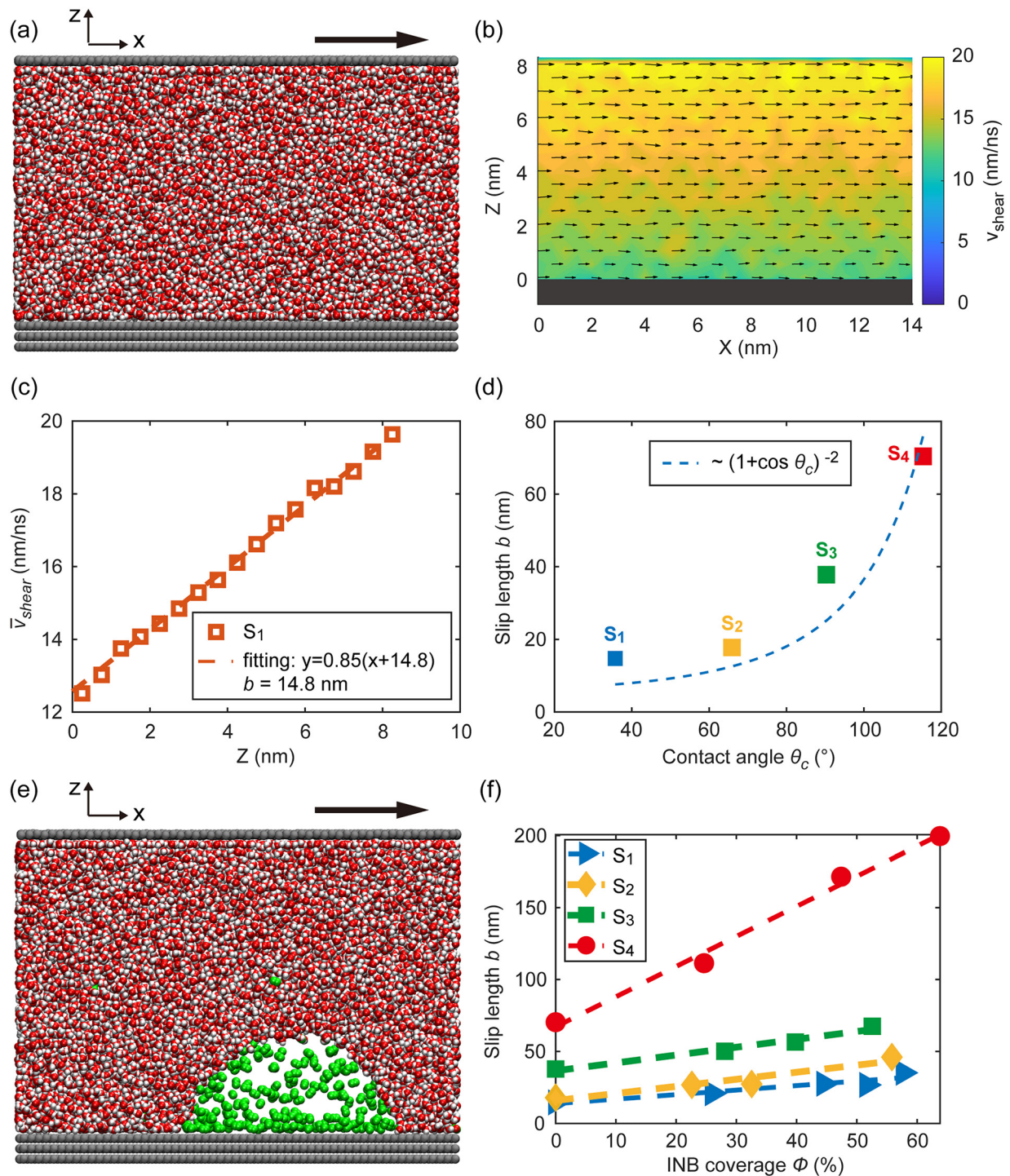
FIG. 1. Boundary conditions on the smooth substrate. (a) The simulation model of the boundary condition on the bare smooth substrate. (b) The water flow field on the S_1 bare smooth substrate. (c) The average shear flow velocity as a function of normal distance Z above the solid–water interface. (d) The slip length as a function of contact angle of the bare smooth substrate. (e) The simulation model of the boundary condition on the smooth substrate with an INB (Multimedia view). (f) The slip length as a function of INB coverage on four substrates with different hydrophobicities. Note: in all snapshots, the silver beads represent solid atoms, the green beads represent gas atoms, and the red and white beads represent oxygen and hydrogen atoms of the water molecule, respectively. Multimedia views: https://doi.org/10.1063/5.0141614.1; https://doi.org/10.1063/5.0141614.2

TABLE I. Simulation parameters of each atom type.

Atoms	σ	ε	Charge (e)
S_T	0.3190	1.0000	0
S_1	0.3190	0.5700	0
S_2	0.3190	0.3920	0
S_3	0.3190	0.2500	0
S_4	0.3190	0.1000	0
S_5	0.3190	0.0615	0
O_W	0.3166	0.6502	−0.8476
H_W	0	0	+0.4238
N	0.3261	0.2887	0

The simulation time lasted 20 ns. The substrate atoms were fixed throughout the whole simulation process.

Following the equilibrium stage, the production simulation began. In this stage, the z-directional position of the upper slab was fixed, and a rightward pulling force was used to make the top slab move rightward at a fixed velocity of 20.0 nm/ns [see Fig. 1(a)]. As the gas molecules can move freely, some gas molecules dissolve in the water phase, even nucleate and grow on the upper wall.[46] In this simulation, the upper slab was set as fully hydrophilic, to drive the water flow and avoid the attachment of the bubbles on it. The simulation time was 40 ns. The velocities of each atom must be written to the output trajectory files to allow the following analysis.

C. Data analysis methods

To measure the protrusion angle of the INB, we used a circle function to fit the water–air interface. This interface was identified as the region where the water density is equal to half (45%–55%) of the bulk water density, and we only used bins located at least 0.5 nm above the substrate to avoid density fluctuations near the substrate. The solid–water interface was defined as the position of the top layer of the substrate plus 0.15 nm (about half of the σ_{SL}). We divided the x-z plane of the simulation box into small bins with a size of 0.1×0.1 nm^2 and calculated the density of water molecules in each bin by averaging over 50 simulation snapshots within 0.1 ns. We analyzed 50 protrusion angles of the INB over a period of 5 ns and calculated their average value as the final result.

The flow field was obtained by analyzing the velocity information of the trajectory files. The Shell, Python, and MATLAB scripts were used in this process. First, for each coordinate file, the x-z plane of the box was cut into bins with the size of 1.0 nm (x-direction) × 0.5 nm (z-direction). Then, the water molecules inside each bin were searched (only oxygen atoms were analyzed). For the water molecules inside each bin, their x-directional and z-directional velocities were averaged, respectively. Hence, the averaged x-directional and z-directional velocities of each bin were obtained. For the water flow field, the simulation time was 40 ns, and the period of 10–40 ns was used for analysis. For all the frames within 10–40 ns (15 000 frames), we calculated the averaged velocities of each bin in each frame first and then calculated the average value of each bin from all the frames. So far, we obtained the averaged x-directional and z-directional velocities of each bin from the 15 000 frames. The x-directional velocity was used to draw the color map of the shear velocity. The combination of x-directional and z-directional velocities was used to draw the flow field distribution indicated by the arrows, as shown in Fig. 1(b). For the flow field of gas molecules, considering the much lower density of the gas phase, a longer simulation time is needed to obtain a smooth flow field. Hence, the simulation time was extended to 200 ns, and the period of 10–200 ns was used for obtaining the average velocity.

After obtaining the flow field of the water molecules, we averaged the x-directional velocities of each z-coordinate. Then, the water velocity as a function of Z was obtained [see Fig. 1(c)]. Finally, we fitted the relationship between velocity and distance by an equation of $\bar{v}_{shear} = a(Z + b)$, where $\bar{v}_{shear}$ is the average shear flow velocity, Z is the normal distance above the solid–water interface, and a and b are the fitting parameters. b is defined as slip length. For the simulations with INB, only bins above the bubble were used for the fitting.

III. RESULTS AND DISCUSSION

A. Boundary conditions on the smooth substrate

1. Bare smooth substrate

The simulation model of the boundary condition on the bare smooth substrate is displayed in Fig. 1(a). In this model, we simulated the water shear flow by pulling the top slab rightward at a fixed velocity of 20.0 nm/ns. The top slab surface can be regarded to have no-slip boundary condition due to its ultra-hydrophilic property. As a result, the water molecular layer adjacent to the top slab moves rightward at the same velocity as the slab, which is consistent with the reported results.[54,55] The motion of the top water molecular layer drives the water molecules inside the whole channel to flow rightward. Owing to the frictional drag force from the bottom substrate, the water molecular layer adjacent to the bottom substrate moves slower than the top water molecular layer. Thus, a shear flow velocity gradient occurs between two slabs. As shown in Fig. 1(b), the flow field between the top slab and a given bare smooth substrate (S_1 in Table I) indicates that the shear flow velocity gradually decays from the top to bottom. The shear velocity value is not precisely the same at each Z position, which may be attributed to the small bin size and the 40 ns simulation time, constrained by the current limitations of state-of-the-art computational resources.

The average shear flow velocities $\bar{v}_{shear}$ at different distances Z from the bottom solid–water interface were further extracted, as shown in Fig. 1(c). The shear flow velocity $\bar{v}_{shear}$ decreases linearly with decreasing Z. For $Z = 0$, $\bar{v}_{shear}$ is around 12.5 nm/ns, indicating the slip boundary condition. By further linearly fitting the correlation between $\bar{v}_{shear}$ and Z, we obtained the slip length $b = 14.8$ nm on the S_1 bare smooth substrate. Furthermore, we simulated the boundary conditions on S_2, S_3, and S_4 bare smooth substrates. Figure 1(d) shows the correlation between the slip length on the four applied substrates and their wettabilities, which are indicated by the contact angle of the water droplet. The slip lengths b on S_1, S_2, S_3, and S_4 are 14.8, 17.8, 37.8, and 70.4 nm, respectively. This result indicates that the higher surface hydrophobicity significantly enhances the boundary slip, which is consistent with Ref. 56. The relationship of slip length with contact angle can be fitted by a quasi-universal function $b \sim (1 + \cos \theta_c)^{-2}$ proposed by Huang et al.[57] The simulated slip length is slightly higher than the predicted value from function $b \sim (1 + \cos \theta_c)^{-2}$ when $\theta_c < 90°$, likely due to the high density of adsorption sites that are closely spaced, allowing for easy migration of water molecules from one site to the next. This phenomenon can cause smooth hydrophilic surfaces to exhibit liquid slip.[58,59]

2. Smooth substrate with an INB

We simulated the boundary condition on a smooth substrate with an INB sitting on it, as shown in Fig. 1(e) (Multimedia view). Four substrates with different wettabilities (S_1, S_2, S_3, and S_4 in Table I) were applied, and the INB coverage was tuned from 0% to 60%. In this model, INB coverage was the ratio of the contact area of the INB to the surface area of the substrate. The slip length on the four employed substrates with different INB coverages is shown in Fig. 1(f). The slip length b linearly increases with increasing INB coverage ϕ for all substrates. The slope of the linear relation between b and ϕ increases with the hydrophobicity of the substrate. On the smooth surface, the water flow drives the INB to move rightward without the pinning effect. Considering that the friction drag between the INB and substrate can be neglected compared with that between water and substrate, a broader INB coverage corresponds to a smaller friction drag. This may be the reason for the enhanced slip length with increasing INB coverage on a smooth surface.

B. Boundary conditions on the rough substrate

1. Bare rough substrate

Rough substrates are universal in practical applications. From this section, we will investigate the boundary conditions on the rough substrates. Figure 2(a) (Multimedia view) shows the simulation model of the boundary slip on the bare rough substrate. A groove with length $L = 4.75$ nm and depth $H = 0.67$ nm was configured in the substrate to simulate the roughness. Here, we set the substrate as Wenzel wetting state, i.e., no INB being trapped in the groove. The flow field on the bare rough substrate (S_3 in Table I) is shown in Fig. 2(b). The shear flow velocity near the bottom substrate is much slower than that near the top slab. We noticed that water molecules in the groove barely flow, which produces drag forces on the molecules over the groove. These drag forces reduce the shear flow velocity near the bottom.

The average shear flow velocities $\bar{v}_{shear}$ at different distances Z from the bottom solid–water interface for four different bare rough
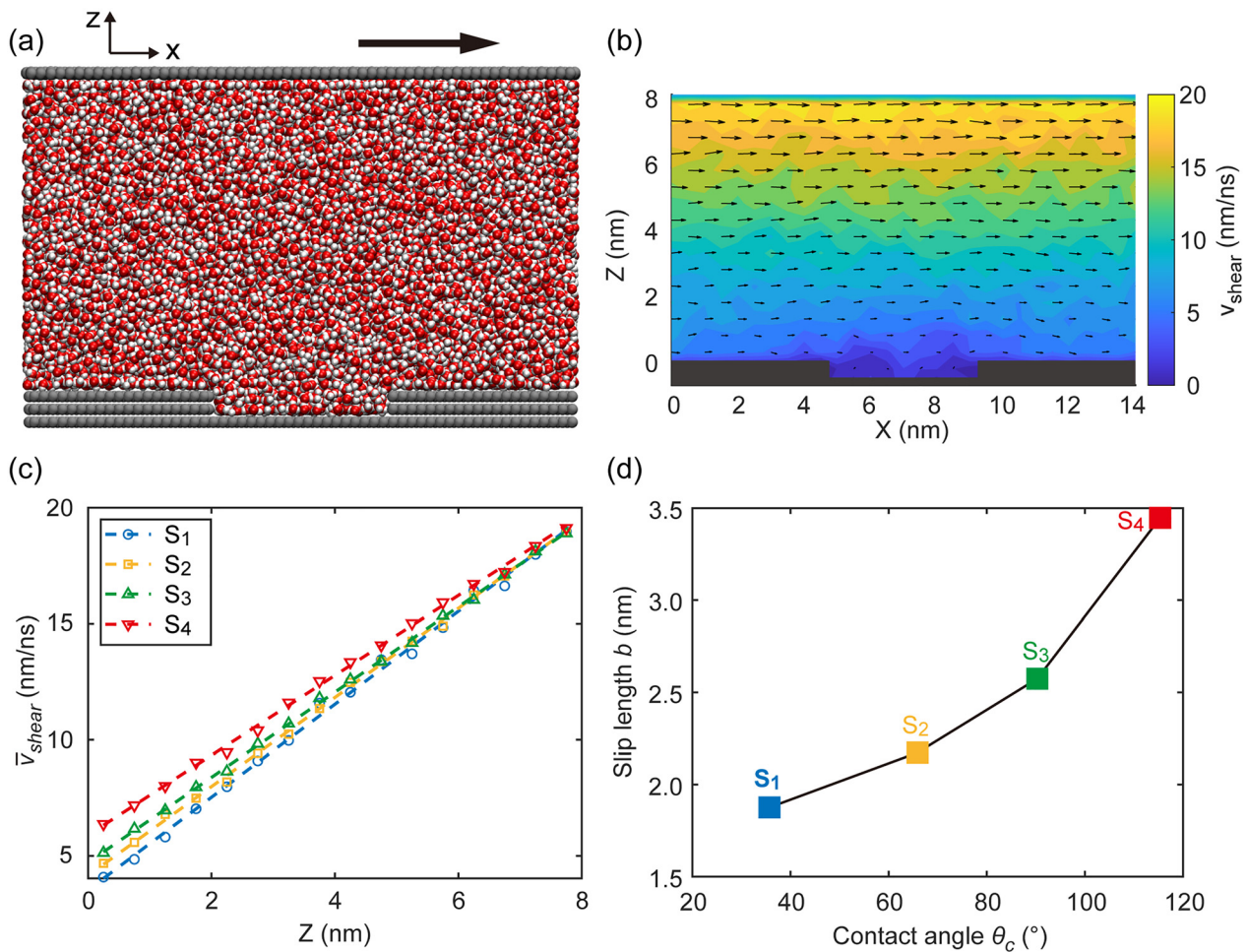

FIG. 2. Boundary conditions on the bare rough substrate. (a) The simulation model of the boundary condition on the bare rough substrate. (b) The water flow field on the rough bare substrate (S_3). (c) The shear flow velocity as a function of Z (normal distance above the solid–liquid interface) on four bare rough substrates (S_1, S_2, S_3, and S_4). (d) The slip length as a function of the contact angle of the bare rough substrate. Note that the contact angle here represents the contact angle of a water drop on the smooth substrate with the same solid–liquid interaction parameters. Multimedia view: https://doi.org/10.1063/5.0141614.3

substrates (S_1, S_2, S_3, and S_4) are shown in Fig. 2(c). When Z decreases from 8 nm to 0, $\bar{v}_{shear}$ decreases from around 20 to around 5 nm/ns, which is much slower than that on the bare smooth substrate [12.5 nm/ns, Fig. 1(c)]. The corresponding slip lengths b on four bare rough substrates (S_1, S_2, S_3, and S_4) are 1.9, 2.2, 2.6, and 3.4 nm, respectively, as shown in Fig. 2(d). Thus, on the bare rough substrates, the slip length b increases with the surface hydrophobicity, which is similar to the bare smooth substrates. However, with the same surface hydrophobicity, the slip length b on the bare rough substrate is shorter than that on the bare smooth substrate by more than an order of magnitude.

2. Rough substrate with an INB

INBs can be trapped on grooves in nanoscale and keep a long-term stability.[60] Here, we studied the boundary conditions on the rough substrates with trapped INBs. In Figs. 3(a) and 3(b) (Multimedia views), we show the simulation models of the boundary conditions on the rough substrate (S_3) with INBs trapped by the grooves. The protrusion angles θ_p in Figs. 3(a) and 3(b) are 25° and 54°, respectively. Figures 3(c) and 3(d) show the water flow field corresponding to Figs. 3(a) and 3(b), respectively. The water flows around the top surface of the INB rather than being dragged by the groove [Fig. 2(b)]. The average shear flow velocities $\bar{v}_{shear}$ at different distances Z are extracted from Figs. 3(c) and 3(d), as shown in Fig. 3(e). When Z decreases from 8 nm to 0, $\bar{v}_{shear}$ decreases from 20 nm/ns to 9.5 nm/ns for $\theta_p = 25°$ and from 20 to 2.5 nm/ns for $\theta_p = 54°$.

We simulated the boundary conditions on four substrates (S_1, S_2, S_3, and S_4) with trapped INBs with different protrusion angles θ_p from around 15° to 82°. Here, we defined slip length increment Δb as the difference between the slip length b on a substrate with a trapped INB and the same substrate without INB. As shown in Fig. 3(f), for all given substrates, Δb decreases with the increase in the θ_p of the trapped INB. All data points of the relation between Δb and θ_p converge into one curve, suggesting that the dependence of the Δb on the θ_p is barely affected by the wettability of the substrate within the employed space of θ_p. In addition, when $\theta_p \lesssim 50°$, $\Delta b > 0$, corresponding to an enhancement of slip length by INBs. In contrast, when $\theta_p \gtrsim 50°$, $\Delta b < 0$, demonstrating that the INBs inhibit the boundary slip.

The INBs inside the grooves have two main effects on the water flow in the channel. On the one hand, INBs shield the interaction between the groove and water in the channel, strongly reducing the drag effect from the groove on the water flow. On the other hand, INBs with larger protrusion angles θ_p increase the surface roughness, producing an increasing drag from the INBs on the water flow. Thus, the competition between these two effects from INBs determines the enhancement or the inhibition of the boundary slip. This result supports previous experimental observations that INBs always increase the slip length.[39,43,61,62] The reason is that the protrusion angles of INBs in experiments are usually lower than 30°.[26–28]

C. Controlling the boundary conditions by INB quantity

In this section, we further investigate the dependence of boundary slip on INB quantity. Figure 4(a) shows the simulation models of the boundary conditions on rough substrates with one INB and three INBs. In these models, the INB coverage was fixed at $\phi = 50\%$, and the protrusion angles θ_p of the INBs are tuned from around 10° to

72°. As shown in Fig. 4(d), for the case of one INB, the slip length b decreases from 14.3 nm to −1.7 nm when the θ_p is from 17° to 70°. For three INBs, the b decreases from 6.7 nm to −0.3 nm when the θ_p is from 10° to 72°. Moreover, we find that when $\theta_p \lesssim 55°$, b for one INB is longer than that for three INBs. When $\theta_p \gtrsim 55°$, b for one INB is shorter than that for three INBs. Thus, even with the same coverage ϕ and the protrusion angle θ_p of INBs, the slip length b can be controlled by adjusting the quantity of INBs.

Figure 4(b) shows the simulation models for no INB, one, and two INBs trapped inside the grooves with Cassie–Baxter wetting state. The diameters and protrusion angles θ_p of all INBs are around 5 nm and 10°. Figure 4(e) (blue squares) plots the slip length b for no INB, one, two and three INBs, which have the same θ_p and diameter. The corresponding values of b are 19.9, 13.1, 8.6, and 6.7 nm, respectively. We find that the slip length b decreases with increasing INB quantity, which is caused by the involved grooves and the trapped INBs reducing the coverage of the smooth surface.

For one substrate with a specific groove quantity, we investigated the boundary conditions with different quantities of trapped INBs, i.e., the mixing of Cassie–Baxter and Wenzel wetting state. The simulations models for no INB, one, two, and three trapped INBs on the substrate with three grooves are shown in Figs. 4(c) and 4(a-II). Figure 4(e) (orange circles) plots the slip length b for no INB, one, two, and three INBs. The corresponding values of b are 1.0, 1.9, 3.5, and 6.7 nm, which increase with increasing INB quantity. This result is consistent with that in Sec. III B 2, namely, that the INBs with small protrusion angle θ_p can enhance the slip length b by shielding the interaction between the water and grooves.

D. Dependence of the boundary condition on INB fluidity

To find out the mechanism by which INBs enhance slip length, we simulated the flow field inside the trapped INB. As shown in Fig. 5(a), a circulation flow of gas molecules was observed inside the INB, indicating a high fluidity of the gas molecules. The annular flow of gas is caused by the tangential viscous stress exerted by the surrounding water flow on the gas bubble. Subsequently, we investigated the role of the fluidity of gas molecules in the boundary slip enhancement by fully constraining the gas fluidity inside the INB. Figure 5(b) displays the comparison of slip length b between the substrates with free INB and frozen INB for the protrusion angle of $\theta_p = 17°$, 36°, 42°, and 66°. The free INB corresponds to the original INB, in which the gas molecules move freely. The frozen INBs represent the bubble in which the fluidity of gas molecules is constrained. The slip length b strongly decreases after freezing the gas molecules inside the INBs. Compared with the bare rough substrate, only in the case of $\theta_p = 17°$, the frozen INB can enhance the boundary slip. Thus, we are convinced that the fluidity of the gas molecules inside the INB dominates the boundary slip enhancement.

IV. CONCLUSIONS

We systematically studied the boundary conditions on solid substrates with INBs by molecular dynamics (MD) simulations. Our results indicate that for smooth substrates, the presence of INBs can enhance boundary slip, and the degree of slip increases with the coverage of INBs. This effect can be attributed to the fact that the INBs decrease the contact area between the solid and water, thereby
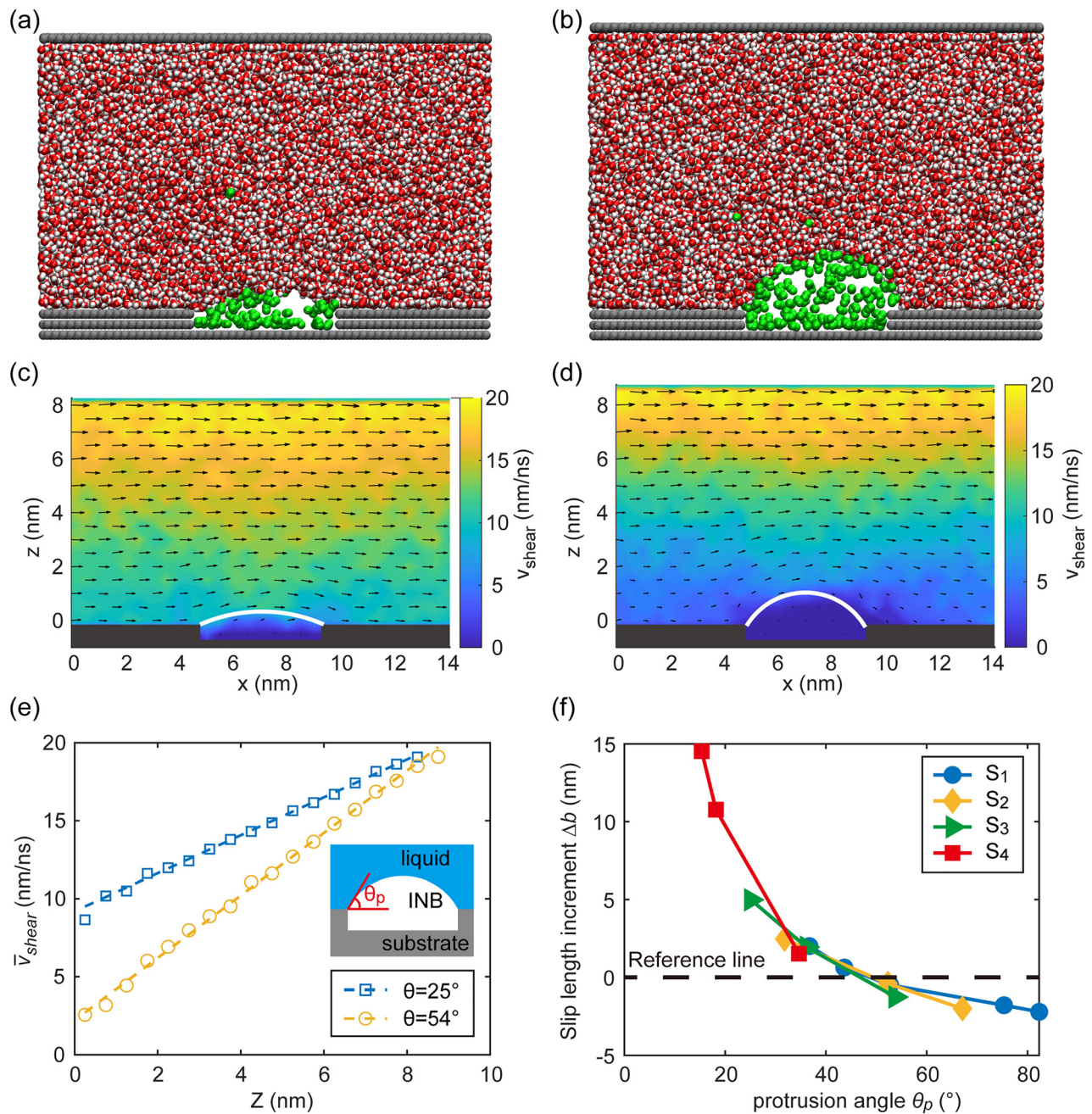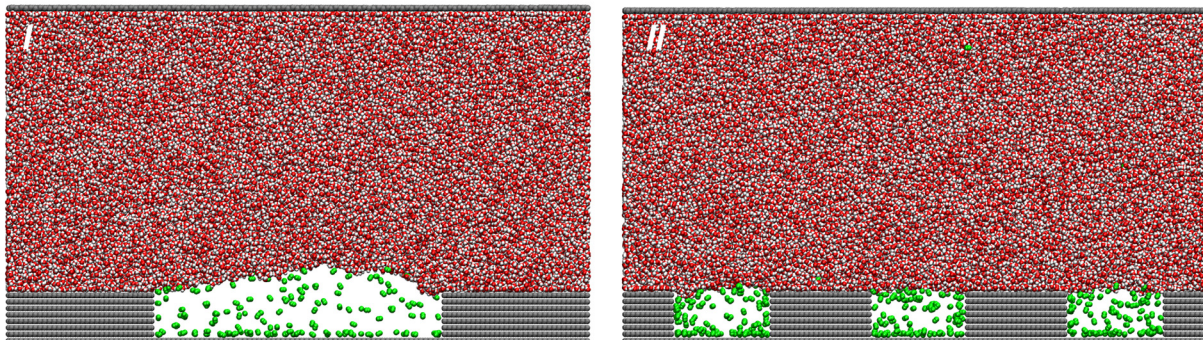
FIG. 3. Boundary conditions on the rough substrate with an INB. (a) and (b) The simulation models of the boundary conditions on the rough substrate (S_3) with a trapped INB with a protrusion angle of 25° (a) and 54°(b), respectively. (c) and (d) The corresponding flow fields for the simulation model in (a) and (b); the white color arc is the surface of the INB for guiding the eye. (e) Average shear flow velocity as a function of Z (normal distance from the solid–water interface) for simulation models in (a) and (b); θ_p in the inset represents the protrusion angle. (f) The increase in slip length Δb on rough substrates (S_1, S_2, S_3, and S_4) with an INB with different protrusion angles. Here, Δb is defined as the difference between the slip length b on a substrate with a trapped INB and the same substrate without INB. Multimedia views: https://doi.org/10.1063/5.0141614.4; https://doi.org/10.1063/5.0141614.5

reducing the frictional drag on the flow of water. For rough substrates that have grooves, the impact of INBs on the boundary conditions is determined by the protrusion angle θ_p. When $\theta_p \lesssim 50°$, INBs shield the interaction between the grooves and water, resulting in an increase

in slip length. However, when $\theta_p \gtrsim 50°$, the presence of INBs restricts the flow of water, leading to a reduction in slip length. Furthermore, we found that the quantity of INBs also plays a role in determining the boundary conditions. For the same INB coverage and protrusion

(a) with the same INB coverage

(b) Cassie-Baxter wetting state
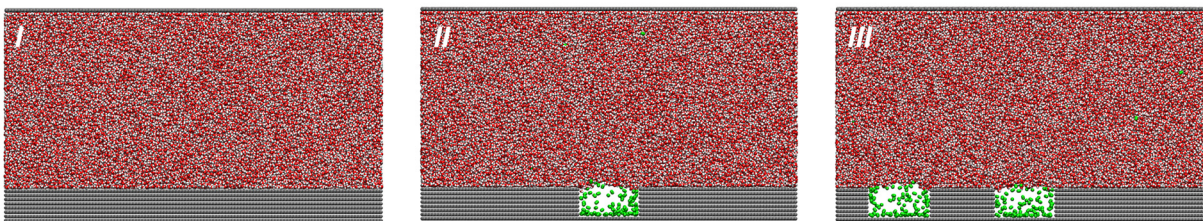
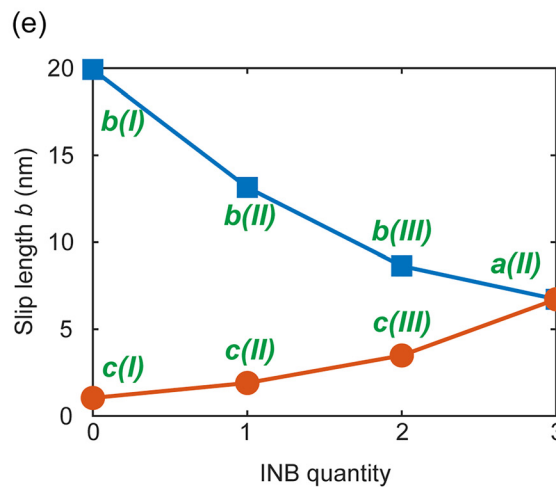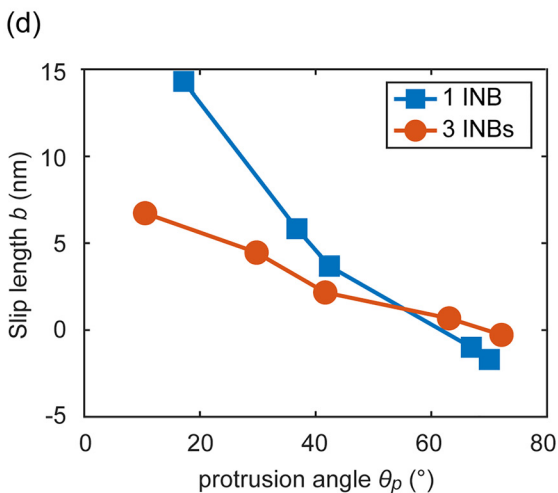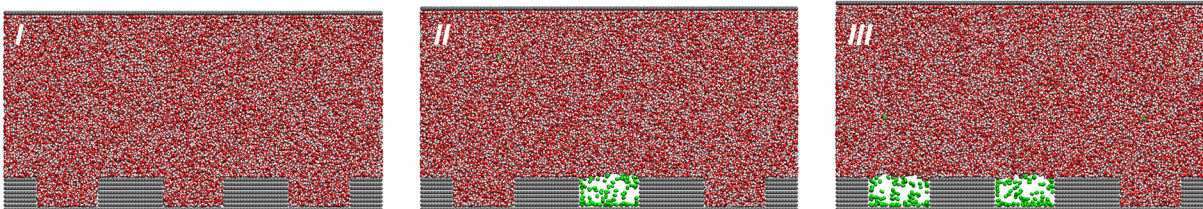**(c) Wenzel + Cassie-Baxter wetting state**

(d)

(e)

FIG. 4. Boundary conditions on rough substrate (S_2) influenced by INB quantity. (a) Simulation models of the boundary conditions on rough substrates with one INB (I) and three INBs (II). The INBs coverages are fixed at 50%. (b) Simulation models of the boundary conditions on rough substrates with zero (I), one (II), and two (III) INBs trapped by grooves, i.e., Cassie–Baxter wetting state. (c) Simulation models of the boundary conditions on rough substrates with zero (I), one (II), and two (III) INBs, where the total grooves number is three. The grooves without INBs are wet by water molecules (Wenzel wetting state). (d) The slip length on rough substrates with one INB and three INBs with different protrusion angles. (e) The slip length as a function of INB quantity for two different wetting states.
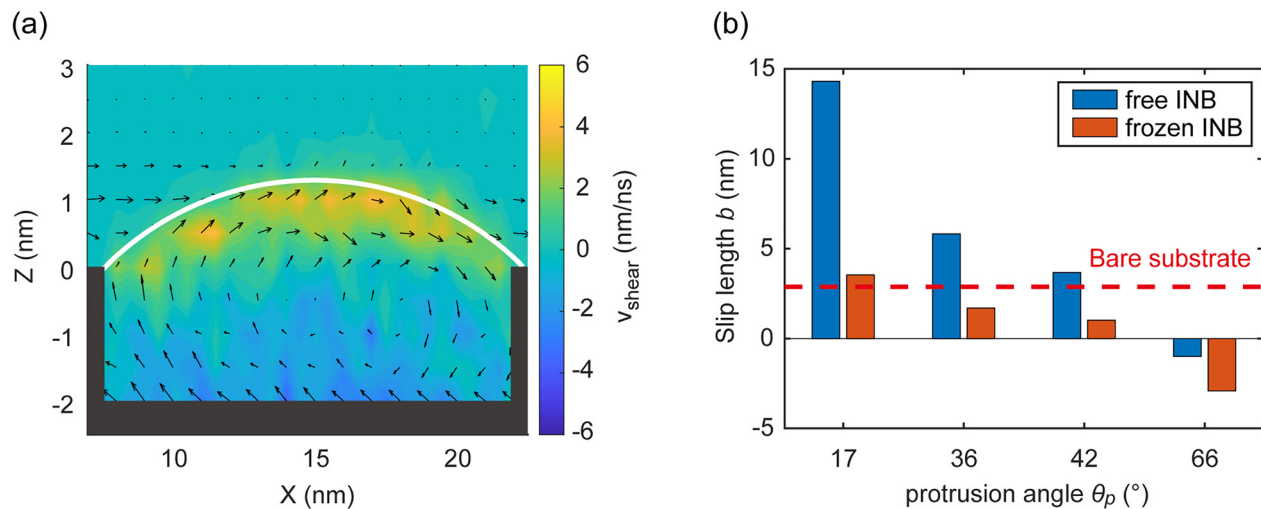
05 March 2024 21:24:22

FIG. 5. The influence of gas fluidity on boundary conditions. (a) The flow field of gas molecules inside the INB. (b) The comparison of slip length between free INB and frozen INB with four different protrusion angles θ_p.

angle, a smaller quantity of INBs is more effective in increasing slip length when $\theta_p \lesssim 55°$. In contrast, when $\theta_p \gtrsim 55°$, a smaller quantity of INBs suppresses boundary slip more effectively. For INBs with fixed size and low protrusion angle of $\theta_p = 10°$, the slip length decreases with an increase in INB quantity when all grooves are covered by INBs (Cassie–Baxter wetting state). However, the slip length increases with an increase in INB quantity for the same surface structure, where the number of grooves is fixed and only some grooves are covered by INBs (Wenzel + Cassie–Baxter wetting state). Additional studies revealed that internal gas molecules circulate inside the INBs. By freezing the gas molecules inside the INBs, we found that the slip length significantly decreases, demonstrating that the high fluidity of gas molecules inside the INBs is the dominant factor contributing to the enhancement of boundary slip caused by INBs.

Our findings provide further insight into the fundamental understanding of boundary slip enhancement triggered by INBs and suggest a promising approach to manipulate the boundary conditions using INBs.

AUTHOR DECLARATIONS
Conflict of Interest

The authors have no conflicts to disclose.

Author Contributions

Haichang Yang and Binglin Zeng contributed equally to this work.

Haichang Yang: Conceptualization (equal); Data curation (equal); Formal analysis (equal); Software (equal); Writing – original draft (equal). **Binglin Zeng:** Formal analysis (equal); Methodology (equal); Visualization (equal); Writing – review & editing (equal). **Xuehua Zhang:** Formal analysis (equal); Methodology (equal); Writing – review & editing (equal). **Yaowen Xing:** Conceptualization (equal); Formal analysis (equal); Methodology (equal); Supervision (equal); Writing – review & editing (equal). **Xiahui Gui:** Methodology (equal); Writing – review & editing (equal). **Yijun Cao:** Conceptualization (equal); Supervision (equal); Writing – review & editing (equal).

DATA AVAILABILITY

The data that support the findings of this study are available from the corresponding authors upon reasonable request.

REFERENCES

[1] C. Tropea, A. L. Yarin, and F. John, *Springer Handbook of Experimental Fluid Mechanics* (Springer, Berlin, 2007).

[2] C. Vega-Sánchez, S. Peppou-Chapman, L. Zhu, and C. Neto, "Nanobubbles explain the large slip observed on lubricant-infused surfaces," Nat. Commun. **13**, 351 (2022).

[3] J. P. Rothstein, "Slip on superhydrophobic surfaces," Annu. Rev. Fluid Mech. **42**, 89–109 (2010).

[4] E. Bonaccurso, H.-J. Butt, and V. S. Craig, "Surface roughness and hydrodynamic boundary slip of a Newtonian fluid in a completely wetting system," Phys. Rev. Lett. **90**, 144501 (2003).

[5] C. Neto, V. Craig, and D. Williams, "Evidence of shear-dependent boundary slip in Newtonian liquids," Eur. Phys. J. E **12**, 71–74 (2003).

[6] L. Li, J. Zhu, S. Zhi, E. Liu, G. Wang, Z. Zeng, W. Zhao, and Q. Xue, "Study of adhesion and friction drag on a rough hydrophobic surface: Sandblasted aluminum," Phys. Fluids **30**, 071903 (2018).

[7] C. Cottin-Bizonne, B. Cross, A. Steinberger, and E. Charlaix, "Boundary slip on smooth hydrophobic surfaces: Intrinsic effects and possible artifacts," Phys. Rev. Lett. **94**, 056102 (2005).

[8] Y. Zhu and S. Granick, "Rate-dependent slip of Newtonian liquid at smooth surfaces," Phys. Rev. Lett. **87**, 096105 (2001).

[9]Y. Kurotani and H. Tanaka, "A novel physical mechanism of liquid flow slippage on a solid surface," Sci. Adv. **6**, eaaz0504 (2020).

[10]D. C. Tretheway and C. D. Meinhart, "Apparent fluid slip at hydrophobic microchannel walls," Phys. Fluids **14**, L9–L12 (2002).

[11]J. Ou and J. P. Rothstein, "Direct velocity measurements of the flow past drag-reducing ultrahydrophobic surfaces," Phys. Fluids **17**, 103606 (2005).

[12]J. Ou, B. Perot, and J. P. Rothstein, "Laminar drag reduction in microchannels using ultrahydrophobic surfaces," Phys. Fluids **16**, 4635–4643 (2004).

[13]S. Calgaroto, K. Wilberg, and J. Rubio, "On the nanobubbles interfacial properties and future applications in flotation," Miner. Eng. **60**, 33–40 (2014).

[14]Y. Xing, X. Gui, L. Pan, B.-E. Pinchasik, Y. Cao, J. Liu, M. Kappl, and H.-J. Butt, "Recent experimental advances for understanding bubble-particle attachment in flotation," Adv. Colloid Interface Sci. **246**, 105–132 (2017).

[15]J. Ryu, H. Byeon, S. J. Lee, and H. J. Sung, "Flapping dynamics of a flexible plate with navier slip," Phys. Fluids **31**, 091901 (2019).

[16]B. Suleimanov, K. F. Azizov, and E. Abbasov, "Slippage effect during gassed oil displacement," Energy Sour. **18**, 773–779 (1996).

[17]B. Suleimanov, "Mechanism of slip effect in gassed liquid flow," Colloid J. **73**, 846–855 (2011).

[18]B. A. Suleimanov, E. F. Veliyev, and V. Vishnyakov, *Nanocolloids for Petroleum Engineering: Fundamentals and Practices* (John Wiley & Sons, 2022).

[19]M. Smith, "Fracture of jammed colloidal suspensions," Sci. Rep. **5**, 14175 (2015).

[20]C. Navier, "Mémoire sur les lois du mouvement des fluides," Mémoires Acad. R. Sci. Inst. France **6**, 389–440 (1823).

[21]C. Wang, Y. Lu, D. Feng, J. Zhou, Y. Li, and H. Zhang, "Experimental study on nanobubble distribution control method based on the slip drag reduction effect," Tribol. Int. **177**, 107940 (2023).

[22]H. Zuo, F. Javadpour, S. Deng, and H. Li, "Liquid slippage on rough hydrophobic surfaces with and without entrapped bubbles," Phys. Fluids **32**, 082003 (2020).

[23]O. Schnitzer, "Slip length for longitudinal shear flow over an arbitrary-protrusion-angle bubble mattress: The small-solid-fraction singularity," J. Fluid Mech. **820**, 580–603 (2017).

[24]D. Li, Y. Wang, Y. Pan, and X. Zhao, "Measurements of slip length for flows over graphite surface with gas domains," Appl. Phys. Lett. **109**, 151602 (2016).

[25]E. Karatay, A. S. Haase, C. W. Visser, C. Sun, D. Lohse, P. A. Tsai, and R. G. Lammertink, "Control of slippage with tunable bubble mattresses," Proc. Natl. Acad. Sci. U. S. A. **110**, 8422–8426 (2013).

[26]W. A. Ducker, "Contact angle and stability of interfacial nanobubbles," Langmuir **25**, 8907–8910 (2009).

[27]D. Lohse and X. Zhang *et al.*, "Surface nanobubbles and nanodroplets," Rev. Mod. Phys. **87**, 981 (2015).

[28]N. D. Petsev, L. G. Leal, and M. S. Shell, "Universal gas adsorption mechanism for flat nanobubble morphologies," Phys. Rev. Lett. **125**, 146101 (2020).

[29]H. Zhang and X. Zhang, "Size dependence of bubble wetting on surfaces: Breakdown of contact angle match between small sized bubbles and droplets," Nanoscale **11**, 2823–2828 (2019).

[30]H. An, B. H. Tan, Q. Zeng, and C.-D. Ohl, "Stability of nanobubbles formed at the interface between cold water and hot highly oriented pyrolytic graphite," Langmuir **32**, 11212–11220 (2016).

[31]J. Qian, V. S. Craig, and M. Jehannin, "Long-term stability of surface nanobubbles in undersaturated aqueous solution," Langmuir **35**, 718–728 (2019).

[32]B. H. Tan, H. An, and C.-D. Ohl, "Stability, dynamics, and tolerance to undersaturation of surface nanobubbles," Phys. Rev. Lett. **122**, 134502 (2019).

[33]L. Zhou, X. Wang, H.-J. Shin, J. Wang, R. Tai, X. Zhang, H. Fang, W. Xiao, L. Wang, C. Wang *et al.*, "Ultrahigh density of gas molecules confined in surface nanobubbles in ambient water," J. Am. Chem. Soc. **142**, 5583–5593 (2020).

[34]S. Wang, L. Zhou, X. Wang, C. Wang, Y. Dong, Y. Zhang, Y. Gao, L. Zhang, and J. Hu, "Force spectroscopy revealed a high-gas-density state near the graphite substrate inside surface nanobubbles," Langmuir **35**, 2498–2505 (2019).

[35]W. Chun-Lei, L. Zhao-Xia, L. Jing-Yuan, X. Peng, H. Jun, and F. Hai-Ping, "High density gas state at water/graphite interface studied by molecular dynamics simulation," Chin. Phys. B **17**, 2646 (2008).

[36]O. I. Vinogradova, "Drainage of a thin liquid film confined between hydrophobic surfaces," Langmuir **11**, 2213–2220 (1995).

[37]O. I. Vinogradova, "Slippage of water over hydrophobic surfaces," Int. J. Miner. Process. **56**, 31–60 (1999).

[38]C. Schönecker, T. Baier, and S. Hardt, "Influence of the enclosed fluid on the flow over a microstructured surface in the Cassie state," J. Fluid Mech. **740**, 168–195 (2014).

[39]Y. Wang, B. Bhushan, and A. Maali, "Atomic force microscopy measurement of boundary slip on hydrophilic, hydrophobic, and superhydrophobic surfaces," J. Vac. Sci. Technol. A **27**, 754–760 (2009).

[40]D. Li, D. Jing, Y. Pan, B. Bhushan, and X. Zhao, "Study of the relationship between boundary slip and nanobubbles on a smooth hydrophobic surface," Langmuir **32**, 11287–11294 (2016).

[41]G. Bolognesi, C. Cottin-Bizonne, and C. Pirat, "Evidence of slippage breakdown for a superhydrophobic microchannel," Phys. Fluids **26**, 082004 (2014).

[42]A. M. Davis and E. Lauga, "Geometric transition in friction for flow over a bubble mattress," Phys. Fluids **21**, 011701 (2009).

[43]A. Steinberger, C. Cottin-Bizonne, P. Kleimann, and E. Charlaix, "High friction on a bubble mattress," Nat. Mater. **6**, 665–668 (2007).

[44]T.-H. Yen, "Effects of wettability and interfacial nanobubbles on flow through structured nanochannels: An investigation of molecular dynamics," Mol. Phys. **113**, 3783–3795 (2015).

[45]H. Zhang, Z. Zhang, and H. Ye, "Molecular dynamics-based prediction of boundary slip of fluids in nanochannels," Microfluid. Nanofluid. **12**, 107–115 (2012).

[46]Y. Lu, "Drag reduction by nanobubble clusters as affected by surface wettability and flow velocity: Molecular dynamics simulation," Tribol. Int. **137**, 267–273 (2019).

[47]Z. Guo and X. Zhang, "Enhanced fluctuation for pinned surface nanobubbles," Phys. Rev. E **100**, 052803 (2019).

[48]C. Cottin-Bizonne, J.-L. Barrat, L. Bocquet, and E. Charlaix, "Low-friction flows of liquid at nanopatterned interfaces," Nat. Mater. **2**, 237–240 (2003).

[49]M. J. Abraham, T. Murtola, R. Schulz, S. P'ąll, J. C. Smith, B. Hess, and E. Lindahl, "GROMACS: High performance molecular simulations through multi-level parallelism from laptops to supercomputers," SoftwareX **12**, 19–25 (2015).

[50]W. Humphrey, A. Dalke, and K. Schulten, "VMD: Visual molecular dynamics," J. Mol. Graph. **14**, 33–38 (1996).

[51]H. Peng, G. R. Birkett, and A. V. Nguyen, "Origin of interfacial nanoscopic gaseous domains and formation of dense gas layer at hydrophobic solid–water interface," Langmuir **29**, 15266–15274 (2013).

[52]H. Yang, Y. Xing, F. Zhang, X. Gui, and Y. Cao, "Contact angle and stability of interfacial nanobubble supported by gas monolayer," Fundam. Res. (published online) (2022).

[53]L. Martínez, R. Andrade, E. G. Birgin, and J. M. Martínez, "Packmol: A package for building initial configurations for molecular dynamics simulations," J. Comput. Chem. **30**, 2157–2164 (2009).

[54]H. F. Abbasov, "Determination of nanolayer thickness and effective thermal conductivity of nanofluids," J. Dispersion Sci. Technol. **40**, 594–603 (2019).

[55]C.-J. Yu, A. Richter, A. Datta, M. Durbin, and P. Dutta, "Molecular layering in a liquid on a solid substrate: An x-ray reflectivity study," Physica B **283**, 27–31 (2000).

[56]J. Harting, C. Kunert, and H. J. Herrmann, "Lattice Boltzmann simulations of apparent slip in hydrophobic microchannels," Europhys. Lett. **75**, 328 (2006).

[57]D. M. Huang, C. Sendner, D. Horinek, R. R. Netz, and L. Bocquet, "Water slippage versus contact angle: A quasiuniversal relationship," Phys. Rev. Lett. **101**, 226101 (2008).

[58]T. A. Ho, D. V. Papavassiliou, L. L. Lee, and A. Striolo, "Liquid water can slip on a hydrophilic surface," Proc. Natl. Acad. Sci. U. S. A. **108**, 16170–16175 (2011).

[59]A. Martini, A. Roxin, R. Q. Snurr, Q. Wang, and S. Lichter, "Molecular mechanisms of liquid slip," J. Fluid Mech. **600**, 257–269 (2008).

[60]Y. Wang, X. Li, S. Ren, H. T. Alem, L. Yang, and D. Lohse, "Entrapment of interfacial nanobubbles on nano-structured surfaces," Soft Matter **13**, 5381–5388 (2017).

[61]Y. Wang and B. Bhushan, "Boundary slip and nanobubble study in micro/nanofluidics using atomic force microscopy," Soft Matter **6**, 29–66 (2010).

[62]E. Lauga and M. P. Brenner, "Dynamic mechanisms for apparent slip on hydrophobic surfaces," Phys. Rev. E **70**, 026311 (2004).

05 March 2024 21:24:22